Parametric Representation of the Primary Hurricane Vortex. Part II: A New Family of Sectionally Continuous Profiles

H. E. WILLOUGHBY

International Hurricane Research Center, Florida International University, Miami, Florida

R. W. R. DARLING

National Security Agency, Fort George G. Meade, Maryland

M. E. RAHN*

NOAA/AOML/Hurricane Research Division, Miami, Florida

(Manuscript received 5 January 2005, in final form 20 July 2005)

ABSTRACT

For applications such as windstorm underwriting or storm-surge forecasting, hurricane wind profiles are often approximated by continuous functions that are zero at the vortex center, increase to a maximum in the eyewall, and then decrease asymptotically to zero far from the center. Comparisons between the most commonly used functions and aircraft observations reveal systematic errors. Although winds near the peak are too strong, they decrease too rapidly with distance away from the peak. Pressure–wind relations for these profiles typically overestimate maximum winds.

A promising alternative is a family of sectionally continuous profiles in which the wind increases as a power of radius inside the eye and decays exponentially outside the eye after a smooth polynomial transition across the eyewall. Based upon a sample of 493 observed profiles, the mean exponent for the power law is 0.79 and the mean decay length is 243 km. The database actually contains 606 aircraft sorties, but 113 of these failed quality-control screening. Hurricanes stronger than Saffir–Simpson category 2 often require two exponentials to match the observed rapid decrease of wind with radius just outside the eye and slower decrease farther away. Experimentation showed that a fixed value of 25 km was satisfactory for the faster decay length. The mean value of the slower decay length was 295 km. The mean contribution of the faster exponential to the outer profile was 0.10, but for the most intense hurricanes it sometimes exceeded 0.5. The power-law exponent and proportion of the faster decay length increased with maximum wind speed and decreased with latitude, whereas the slower decay length decreased with intensity and increased with latitude, consistent with the qualitative observation that more intense hurricanes in lower latitudes usually have more sharply peaked wind profiles.

1. Introduction

In the first paper of this series (Willoughby and Rahn 2004, hereafter Part I), we showed that the most commonly used analytical representation of hurricane winds' radial structure (Holland 1980) suffers from systematic errors. Comparisons between statistically fitted profiles and nearly 500 tropical cyclones observed by aircraft demonstrated that, although the analytical profiles overestimate the width of the eyewall wind maximum, the wind decreases too rapidly with distance from the maximum both inside and outside the eye. Since variants of Holland's profile are fundamental to applications such as modeling storm surge (Jelesnianski 1967) or windstorm risk (e.g., Vickery and Twisdale 1995), these shortcomings highlight the need for a more realistic alternative.

Tropical cyclones are nearly circular vortices with damaging winds concentrated in and around the eyewall. The geometric center of the clear eye or the stagnation point inside the eye defines a vortex center that

* Deceased.

Corresponding author address: H. E. Willoughby, International Hurricane Research Center, Florida International University, 360 MARC Building, University Park Campus, Miami, FL 33199.
E-mail: hugh.willoughby@fiu.edu

can be tracked objectively. Thus, the center position and intensity, measured in terms of maximum wind or minimum sea level pressure, provide a first-order characterization of tropical cyclones. Indeed, the HURDAT file (Jarvinen et al. 1984), which constitutes the authoritative long-term hurricane climatology, contains exactly that information. The role of "parametric" profiles is to convert position and intensity into a geographical distribution of winds. The Holland profile employs three parameters: maximum wind, radius of maximum wind, and B, an exponent that sets the sharpness of the eyewall wind maximum. A key result of Part I was that, even for an optimally chosen B, the magnitude of the second derivative of the wind with respect to radius is too small near the radius of maximum wind where the profile is concave downward and too large away from the maximum where the profile is concave upward. Here we propose a new family of parametric profiles that do not suffer from these limitations. The profile wind is proportional to a power of radius inside the eye and decays exponentially outside the eye with a smooth transition across the eyewall. Least squares fits of these profiles to the same sample of aircraft observations used in Part I validate them and provide statistical estimates of their parameters. Section 2 of this paper formulates the new family of profiles and describes the least squares fitting procedure. Subsequent sections present profiles with a single outer exponential decay length, and with a superposition of two outer exponentials. Section 5 considers alternative profile formulations and addresses hydrodynamic stability of the fitted vortices. Section 6 summarizes results and draws conclusions.

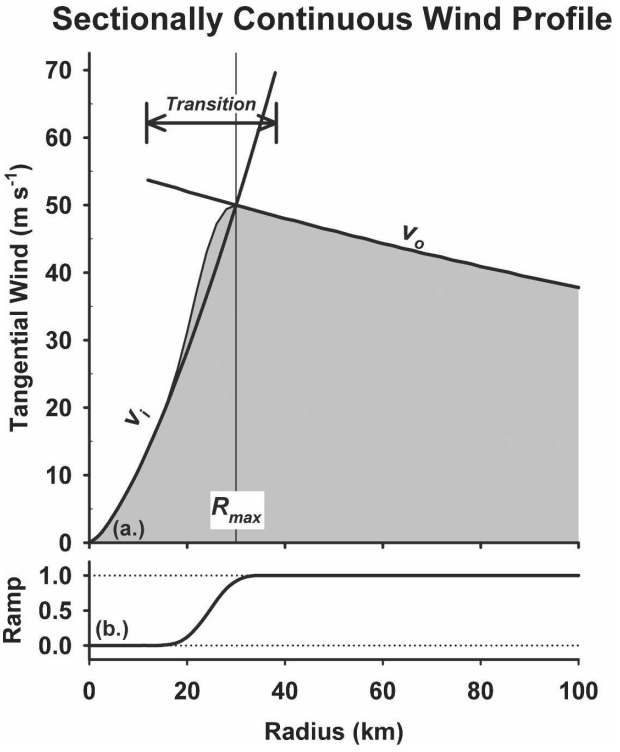

FIG. 1. (a) Schematic illustration of a sectionally continuousù hurricane wind profile (shading) constructed by joining an inner profile with swirling wind proportional to a power of radius and an outer profile with swirling wind decaying exponentially with distance outside the radius of maximum wind (darker curves). (b) In a zone spanning the radius of maximum wind, a polynomial ramp weighting function is used to create a smooth transition between the inner and outer profiles.

2. Analysis

a. Profile formulation

Piecewise continuous wind profiles (e.g., Willoughby 1995) show promise as an alternative to the Holland model. They are composed of analytical segments patched smoothly together (Fig. 1). Inside the eye the wind increases in proportion to a power of radius. Outside the eye, the wind decays exponentially with a radial e-folding distance that changes from storm to storm. The transition across the radius of maximum wind from the inner to outer profiles is accomplished with a smooth, radially varying polynomial ramp function:

$$V(r) = V_i = V_{\max}\left(\frac{r}{R_{\max}}\right)^n, \quad (0 \le r \le R_1), \tag{1a}$$

$$V(r) = V_i(1 - w) + V_o w, \quad (R_1 \le r \le R_2), \tag{1b}$$

$$V(r) = V_o = V_{\max}\exp\left(-\frac{r - R_{\max}}{X_1}\right), \quad (R_2 \le r), \tag{1c}$$

where V_i and V_o are the tangential wind component in the eye and beyond the transition zone, which lies between $r = R_1$ and $r = R_2$; $V_{\max}$ and $R_{\max}$ are the maximum wind and radius at which the maximum wind occurs; X_1 is the exponential decay length in the outer vortex; and n is the exponent for the power law inside the eye. Note that both V_i and V_o are defined throughout the transition zone and that both are equal to $V_{\max}$ at $r = R_{\max}$.

The weighting function, w, is expressed in terms of a nondimensional argument $\xi = (r - R_1)/(R_2 - R_1)$. When $\xi \le 0$, $w = 0$; when $\xi \ge 1$, $w = 1$. In the subdomain $0 \le \xi \le 1$, the weighting is defined as the polynomial

$$w(\xi) = 126\xi^5 - 420\xi^6 + 540\xi^7 - 315\xi^8 + 70\xi^9, \tag{2}$$

which ramps up smoothly from zero to one between R_1 and R_2. As described in the appendix, the weighting function is derived by integration of a bell-shaped polynomial curve given by $C[\xi(1 - \xi)]^k$ when $(0 \le \xi \le 1)$

and zero elsewhere. The coefficient C is chosen to make $w(1) = 1$, and the exponent k is the "order" of the bell and ramp curves, even though the resulting polynomials are of order $2k$ and $2k + 1$, respectively. We have coined the term "bellramp" functions to denote this family of polynomials. Since the shapes of fitted profiles are insensitive to the order of the polynomials, we selected fourth-order ramp functions for smoothness and differentiability.

Based upon parameters $R_{\max}$, $V_{\max}$, X_1, and n, the full wind profile is constructed as follows. First, the width of the transition $R_1 - R_2$ is specified a priori at a value between 10 and 25 km. Then, the location of the transition zone is determined by requiring the radial derivative of (1b) to vanish at $r = R_{\max}$, recognizing that $V_i(R_{\max}) = V_o(R_{\max}) = V_{\max}$. This condition yields the value of w at the wind maximum:

$$w\left(\frac{R_{\max} - R_1}{R_2 - R_1}\right) = \frac{\dfrac{\partial V_i}{\partial r}}{\dfrac{\partial V_i}{\partial r} - \dfrac{\partial V_o}{\partial r}} = \frac{nX_1}{nX_1 + R_{\max}}, \quad (3)$$

which may be solved for R_1 through numerical inversion of (2).

As shown subsequently, in many situations the profile described by (1a)–(1c) suffers from the problem that vexed the Holland profile in Part I. Relatively large values of X_1 chosen to generate profiles that match the outer part of the vortex may fail to capture the rapid decrease of wind just outside the eyewall; conversely, smaller values of X_1 generate profiles that match the steep gradient outside the eyewall and decrease too rapidly farther from the center. Often there is no intermediate value that can fit the observations in both parts of the domain. Although this difficulty is less pronounced than for the Holland profile, it is still problematic. A remedy entails replacement of the single exponential with the sum of two exponentials with e-folding lengths X_1 and X_2:

$$V_o = V_{\max}\left[(1 - A)\exp\left(-\frac{r - R_{\max}}{X_1}\right) + A\exp\left(-\frac{r - R_{\max}}{X_2}\right)\right], \quad (R_1 \le r), \quad (4)$$

where the parameter A sets the proportion of the two exponentials in the profile, and the rightmost expression in (3) becomes $n[(1 - A)X_1 + AX_2]/\{n[(1 - A)X_1 + AX_2] + R_{\max}\}$. Figure 2 illustrates application of (4) to Hurricane Diana of 1984. Clearly, the dual-exponential profile captures the profile's sharpness at the radius of maximum wind as well as the more

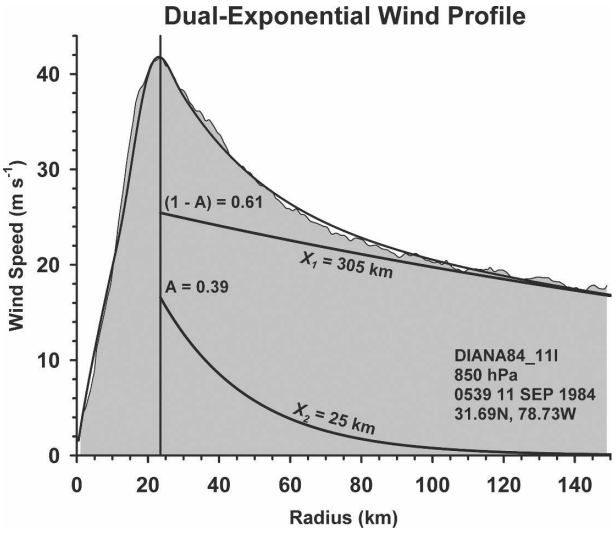

FIG. 2. A dual-exponential profile used to approximate the observed wind in Hurricane Diana on 11 Sep 1984. Here and subsequent shading indicates observed winds, and the darker curves indicate the fitted profiles.

gradual decrease of wind at radii farther from the eyewall. There is an issue of nonuniqueness in this formulation. Several different combinations of X_1, X_2, and A can often fit a given set of observations equally well. This situation complicates statistical estimation of the profile parameters, so that we generally fit A and one variable decay length, keeping the other decay length, usually the shorter one, fixed. Thus, most of this paper will deal with either single-exponential profiles or dual-exponential profiles with one predetermined decay length.

In this formulation, unlike the Holland profile, there is no closed-form relation for the gradient-balance geopotential height in terms of the vortex parameters. Thus, the geopotential height is computed through outward numerical integration of the gradient wind acceleration from the observed height at the vortex center of the standard isobaric surface nearest flight level,

$$Z(r) = Z_c + \frac{1}{g}\int_0^r \left[\frac{V^2(r')}{r'} + fV(r')\right] dr', \quad (5)$$

where $Z(r)$ is the height of the specified surface, Z_c is $Z(0)$, and g is the acceleration of gravity. Setting the upper bound on the integral to infinity in (5) produces a gradient balance estimate of the undisturbed geopotential around the storm, $Z_e = Z(r \to \infty)$. Based upon this integral it is possible to relate $V_{\max}$ to $Z_e - Z_c$ in order to devise height–wind relations for the single-exponential and dual-exponential profiles. A key ad-

vantage of using exponential functions to describe the outer profile is that it guarantees a well-behaved height–wind relationship as well as finite values for vortex total relative angular momentum and kinetic energy.

b. Profile fitting

Single-exponential profiles have four parameters $R_{\max}$, $V_{\max}$, X_1, and n. Dual-exponential profiles with one predetermined decay length have five parameters ($R_{\max}$, $V_{\max}$, X_1, A, and n), and dual-exponential profiles with both decay lengths free have six parameters ($R_{\max}$, $V_{\max}$, X_1, X_2, A, and n). As in Part I, $V_{\max}$ and $R_{\max}$ are determined by scanning each profile for the strongest reported wind and its radial position. This procedure leaves the single-exponential, constrained dual-exponential, and free dual-exponential profiles, respectively, with two, three, and four parameters that require least squares fitting to the data. The cost function is the same as that used in Part I,

$$S^2 = \sum_{k=1}^{K} [v_o(r_k) - v_g(r_k, n, X_1, \ldots)]^2 + g[z_o(r_k) - z(r_k, n, X_1, \ldots)]^2 L_z^{-1}. \quad (6)$$

It is the summed squares of the differences between the profile and observed tangential wind and between the computed geopotential height (5) and the observed height of the isobaric surface nearest the aircraft flight level. Since the parameter space has relatively few dimensions and the cost function is essentially a parabola, we use the simplex algorithm (Nelder and Mead 1965; Press et al. 1986) to find the minimum value of S^2. Here L_z is a Lagrange multiplier that sets the strength of the gradient balance constraint and also makes (6) dimensionally homogeneous with units of velocity squared; we set $L_z = 1$ km, the same value used in Part I.

Ranges of the fitted parameters are constrained with Lagrange multipliers, for example, $0.4 \leq n \leq 2.4$ or $0 \leq A \leq 1$, to prevent the algorithm from wandering into physically unrealistic parts of the parameter space. Typical minimum values of S^2 are a few hundred to a few thousand $m^2\ s^{-2}$, and the penalties imposed outside the preferred subdomain by the Lagrangian constraints are $2–5 \times 10^3\ m^2\ s^{-2}$. The constraints generally have limited effect on the fitted parameters inasmuch as the simplex algorithm almost always finds values within the preferred subdomain. Two exceptions to this generality are $A = 0$ or 1, which characterize profiles where X_1 or X_2 can represent the shape of the "dual exponential" outer profile completely. The constraint on the minimum decay lengths generally is set for values greater than 50–100 km, but the minimization algorithm seldom selects values that small. By contrast, the upper bound on decay lengths does exert significant control over the fitted profiles. In some tropical cyclones where the wind remains fairly constant from just outside the eyewall to the sampling domain boundary, the unconstrained algorithm will seek decay lengths $\geq$1000 km. Since the values of Z_e that result from integration of (5) in these situations may be greater than Z_a, the height of the isobaric surface in climatologically representative soundings (Jordan 1958; Sheets 1969), we generally set an upper bound of a few hundred kilometers on the longer decay length. Tuning of this constraint is discussed extensively in the next two sections, since it is important to obtaining realistic fits.

The data for the least squares fits are the same as those used in Part I. They contain 606 logical sorties into Atlantic and eastern Pacific tropical storms and hurricanes flown by National Oceanic and Atmospheric Administration (NOAA) and Air Force Reserve aircraft between 1977 and 2000 and are representative in terms of geographical and seasonal distribution. They are divided into "logical sorties," each a series of successive transects across the tropical cyclone center at fixed altitude, usually flown by one aircraft during the course of a few hours. Although there are a few sorties with 300-km domains, most extend to $\leq$150 km. The variables are expressed in a cylindrical coordinate system that moves along the objectively determined cyclone track. The observed dynamic and kinematic variables are transformed into vortex-centered coordinates and averaged azimuthally around the vortex to produce a profile composite (PCMP) file for each sortie. The least squares fits use the PCMP files. Predominant flight levels were 850 and 700 hPa (1.5 and 3 km), but some missions (generally in weaker storms) were flown as low as 950 hPa (500 m) and as high as 400 hPa (7 km). Although depressions and weak tropical storms are underrepresented, the sample is reasonably representative in terms of cyclone intensity. Of the original sample, 113 failed quality-control (QC) criteria that screened out profiles where the radius of maximum wind was more than half the sampling domain or where the data fail to describe a well-defined dynamic center inside the eye. The 493 PCMP files that met the QC criteria are homogeneous with the sample used in Part I.

3. Single-exponential profile

The single-exponential profile is the simplest of the new functional forms. Since the Lagrange multiplier constraint on the maximum value of X_1 is the only tun-

ing required, we examine its effect first, by a series of five least squares fits to the entire sample with $X_1 \leq$ 200, 400, 600, 800, and 1000 km (Fig. 3a). The mean value of X_1 increases from 203 to 249 km over this range of upper bounds. For most individual sorties, the constraint has no effect, but for a few the fitting algorithm selects larger values of X_1, increasing the sample average, as the constrained upper bound increases. If one compares the average difference between Z_e, the computed environmental geopotential height from (5), and Z_a, the climatologically expected value, the computed values are always too low, despite the problem with too-large values of X_1 for some sorties. The value of $Z_e - Z_a$ increases from −18.3 m when the constraint requires $X_1 \leq 200$ km to −5.4 m when $X_1 \leq 1000$ (Fig. 3b). Most of the increase happens between $X_1 \leq 200$ km and $X_1 \leq 600$ km. It is important to recognize that the decrease in magnitude of the negative environmental–height bias stems from compensating errors. For most PCMP files, the single-exponential fitting algorithm selects too-small values of X_1 that lead to underestimated values of Z_e. Relaxing the upper constraint on X_1 causes a few PCMP files to produce overestimates of Z_e, which increases the average toward the hoped-for zero bias. For this reason, we set the decay length Lagrange multiplier constraint to $50 \leq X_1 \leq 600$ km, which produces $Z_e - Z_a = -7.4$ m. This value of the constraint produces mean parameters, $n = 0.79 \pm 0.34$ and $X_1 = 243 \pm 141$ km. The mean difference between the fitted and observed winds is essentially zero, and the rms error is 2.5 m s^{-1} (dependant data). The bias and rms errors in geopotential height are 1.3 and 10.4 m. There is a positive Z bias, largely confined inside the 150-km domain where the curve fitting is done. The bias reverses as the integral in (5) is continued beyond 150 km, where V decreases too rapidly with distance from the vortex center.

For Hurricane Anita of 1977 (Fig. 4), chronologically the first tropical cyclone in the database, the fitting algorithm selects $n = 1.16$ and $X_1 = 100.7$ km as the optimum fit. The rms wind and height errors are larger than average for single-exponential profiles, 4.6 m s^{-1} and 18.8 m, respectively, with essentially zero wind bias and 5.4-m positive height bias. Comparison of the wind and geopotential height variations shows a negative height bias due to underestimation of the wind inside the eye. The bias changes over to positive beyond about twice the eye radius because the fitted winds are too strong outside the eye. Farther from the center, the negative height bias decreases in magnitude slowly because the fitted winds are too weak beyond 100-km radius. It is disappointing to see this pattern of errors emerge here because it is similar, though less pronounced, to the one that characterized the Holland profile in Part I.

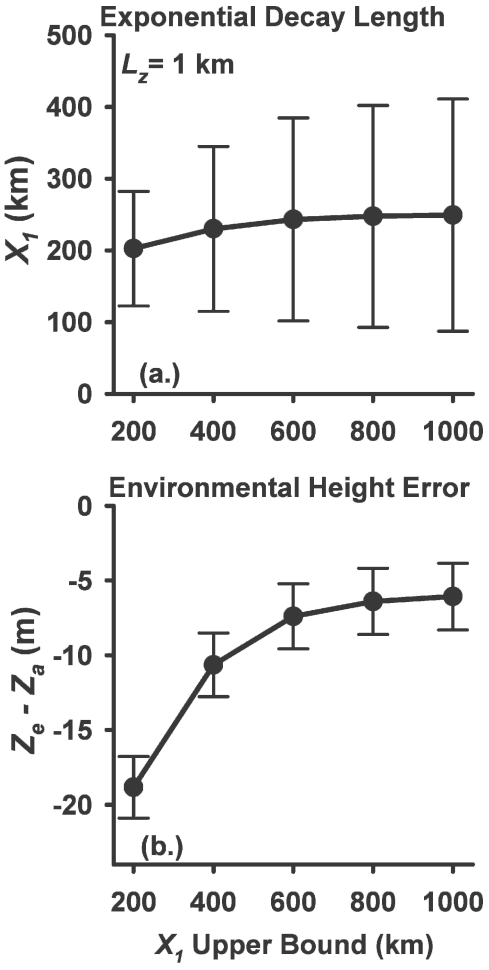

FIG. 3. Variation of (a) outer exponential decay length and (b) difference between computed and climatological environmental geopotential heights as functions of the Lagrange multiplier constraint on the maximum decay length for single-exponential profiles.

The single-exponential profile depicts other tropical cyclones with somewhat more fidelity. In Part I, Hurricane Mitch of 1998 was one of the most successful Holland-profile fits. Here, the single-exponential fit (Fig. 5a, $n = 0.69$, $X_1 = 119$ km) does about as well, although the wind maximum is too narrow. The Holland fit to Hurricane Hugo of 1989 was less successful because the fitted wind maximum was too broad and the wind decreased too rapidly with radius beyond 80 km. The corresponding single-exponential profile (Fig. 5b, $n = 1.67$, $X_1 = 145$ km) fitted both the primary wind maximum and the profile within 120 km of the center closely, but could not represent the outer wind maximum present beyond 120-km radius. Despite improvements with the sectionally continuous fitted profiles,

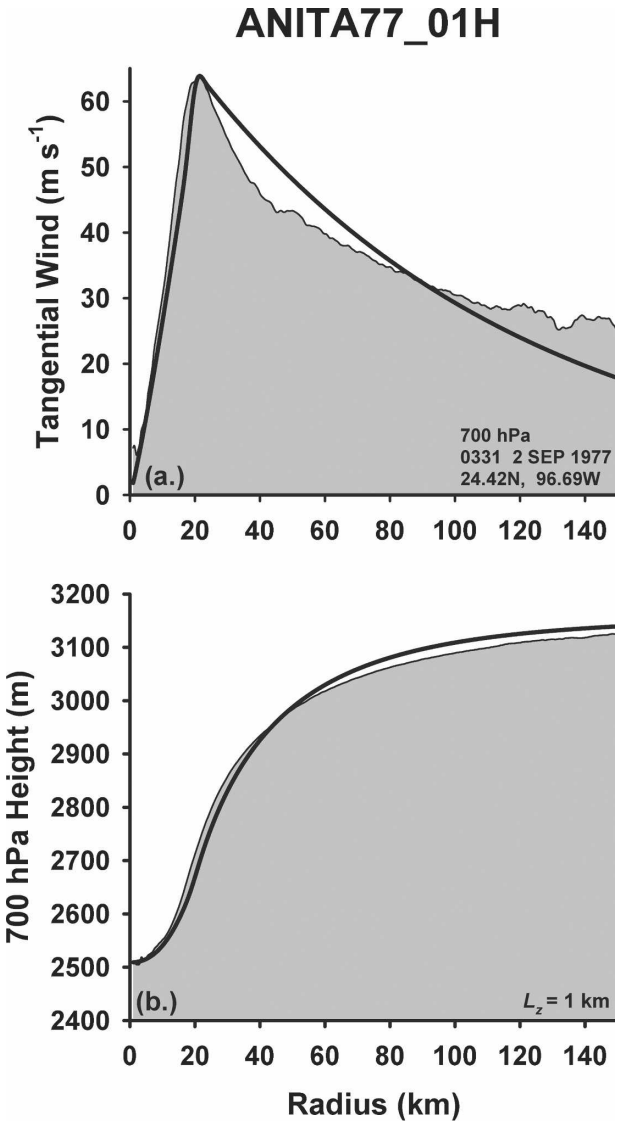

FIG. 4. Single-exponential (a) wind and (b) geopotential height profiles fitted to Hurricane Anita of 1977. Observed and fitted profiles are as indicated in Fig. 2.

both Mitch and Hugo exhibit the same pattern of errors that appeared in Anita and in the Holland profiles.

Edouard of 1996 was another successful Holland profile because its broad wind maximum and gradual decrease of wind outside the eye could be fitted by the Holland profile with a relatively small value of $B = 0.86$. The single-exponential fit (Fig. 5c, $n = 0.41$, $X_1 = 588$ km), with its small exponent inside the eye and long decay length, captures most features of the data except for the broad shoulder of the profile inward from the wind maximum. Erika of 1997 was a relatively unsuccessful Holland fit because the Holland profile was unable to match its sharp wind maximum, even with a relatively large $B = 1.17$. The single-exponential profile (Fig. 5d, $n = 0.581$, $X_1 = 178$ km) was able to represent its shape more accurately. Thus, despite some limitations, the added degrees of freedom here produce significant improvement over the Holland formulation.

Description of hurricane wind profiles in terms of the sample-mean values of n and X_1 misses systematic variations of vortex structure because all four parameters of the single-exponential profile are correlated with each other. A regression line fitted to X_1 decreases from 368 to 86 km as V_{max} increases from 10 to 70 m s^{-1} (Fig. 6a). Over the same interval, n increases from 0.43 to 1.24 (Fig. 6b). Although the slopes of both curves differ from zero at better than 1% significance, there is considerable scatter around the regression lines. In Fig. 6a, the points that cluster near $X_1 = 600$ km and V_{max} between 10 and 42 m s^{-1} have values limited by the Lagrange multiplier constraint, whereas the others are unaffected. Only a few of the n values in Fig. 6b approach the Lagrange multiplier limits. The relatively large values of X_1 found here show that real hurricane vortices are broader than many analytical models used in theoretical studies. This result is consistent with the argument of Mallen et al. (2005) that hurricanes in nature are more resistant to environmental shear than these theoretical arguments lead one to expect.

The means, standard deviations, and the correlation matrix among the parameters (Table 1a) summarize all possible linear relations. As shown in Part I, these statistics contain enough information to prepare linear estimators of the parameters. The eigenvalues and eigenvectors of the correlation matrix (Table 1b) reveal systematic patterns of variation. The leading eigenvector, **E**1, which explains >50% of the parameter standardized variance, delineates increasing n and decreasing X_1 correlated with increasing V_{max}, decreasing latitude, and decreasing ln R_{max}. In qualitative terms, **E**1 depicts shrinking of the eye and sharpening of the eyewall wind maximum with increasing intensity and lower latitude. It is the same physical association as the "convective ring" leading eigenvector in Part I where decreasing R_{max} and increasing B were associated with intensification and lower latitude. In both cases, sharpening of the eyewall wind maximum and shrinking of the eye in more intense hurricanes is consistent with the response of balanced hurricane-like vortices to heating around the eye (Smith 1981; Shapiro and Willoughby 1982; Schubert and Hack 1982). The second eigenvector, **E**2, projects almost entirely onto latitude, associated to some extent with intensity. The qualitative impression is that tropical cyclones in the early and late stages of their life cycles, where intensification through convective heating is either not well established or has run its

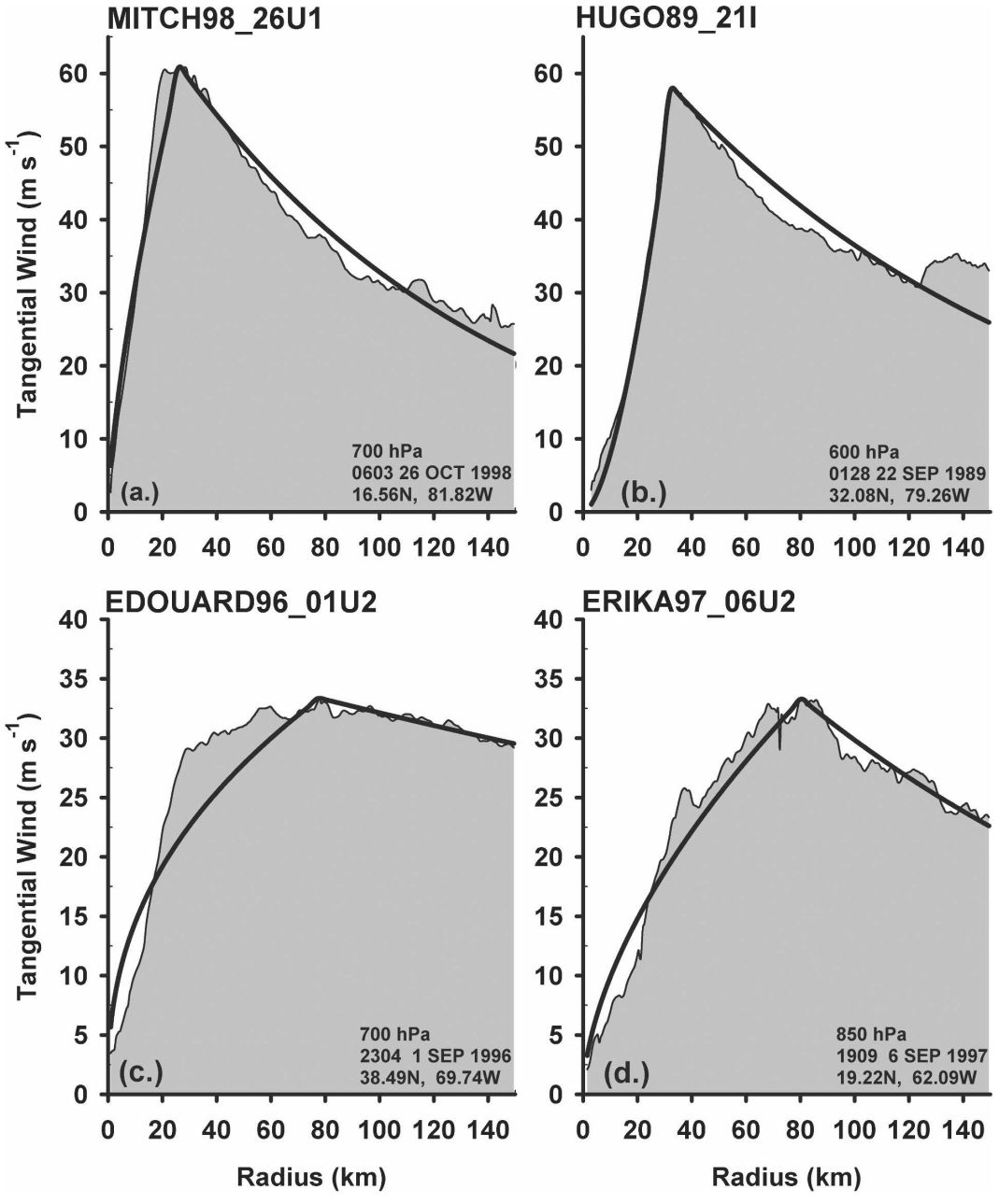

FIG. 5. Single-exponential wind profiles fitted to Hurricanes (a) Mitch of 1998, (b) Hugo of 1989, (c) Edouard of 1996, and (d) Erika of 1997. Observed and fitted profiles are indicated as in Fig. 2.

course, project onto **E**2. Eigenvectors **E**1 and **E**2 combined explain >70% of the standardized parameter variance. It is difficult to advance physical interpretations for the remaining eigenvectors, which together explain <30% of the standardized parameter variance.

As described in Part I, the ratio of the standard, multivariate normal probability density described by the correlation matrix (Table 1a) to the unconditional probability density of V_{max} and φ is the probability density of ln R_{max}, n, and X_1 conditional upon the known values of V_{max} and φ. This last distribution contains linear regression relations for the unknown parameters in terms of the known:

$$R_{max} = 46.4 \exp(-0.0155V_{max} + 0.0169\varphi), \quad (7a)$$

$$X_1 = 270.5 - 4.78V_{max} + 6.176\varphi, \quad (7b)$$

$$n = 0.431 + 0.136V_{max} - 0.006\varphi. \quad (7c)$$

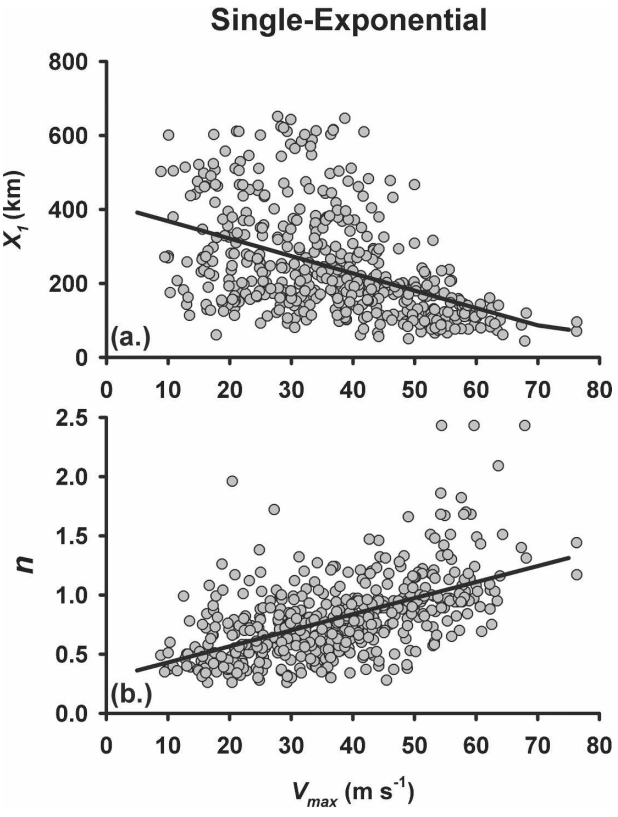

FIG. 6. Scatterplots and regression lines for fitted (a) single-exponential outer decay length and (b) power-law exponent as functions of maximum wind. Shaded circles represent parameter values determined for individual profiles by the fitting algorithm.

All of the coefficients in (7a)–(7c) differ from zero with better than 1% statistical significance. The statistical distribution $R_{\max}$ is skewed toward large values so that it is more nearly lognormal than normal (Part I).

Substitution from (7a)–(7c) into (5) and continuation of the integral to large (1200 km) radius for incrementing values of maximum wind produces a table of $(Z_e - Z_c)$ as a function of $V_{\max}$. Since an algebraic relation between minimum height and maximum wind is more useful than a table, we fit the tabular output with power-law expressions similar to that used by Atkinson and Holliday (1977). For example, at 25°N, the relation between minimum isobaric height and maximum wind is

$$V_{\max} = 0.652(Z_e - Z_c)^{0.724}. \quad (8)$$

This relation takes into account the sharpening of the profile with intensity embodied in **E**1, whereas if one substitutes mean values of $R_{\max}$, n, X_1, and φ into (7a)–(7c), the profiles scale only as $V_{\max}$ so that there is a "universal" height–wind relation with wind proportional to the square root of the height fall:

$$V_{\max} = 2.16\sqrt{Z_e - Z_c}. \quad (9)$$

In Part I, an empirical fit of maximum wind to height fall yielded a similar relation with a coefficient of 2.10, based upon all the PCMP files, including the 113 profiles excluded here because they failed the QC criteria. The next section will deal more completely with the dynamically calculated height–wind relations for dual-exponential profiles.

As in Part I, bootstrap comparisons among subsets of the data provide an assessment of fitted profiles ability to represent independent data. The sample is divided into three subsets, spanning the years 1977–89, 1990–95, and 1996–2000, inclusive. Regression relations analogous to (7a)–(7c) were computed based upon all possible pairs of subsets and used to model the profiles in

TABLE 1. (a) Mean, std dev, and correlation matrix for the single-exponential profile variables computed from the 493 sorties that passed QC screening. For $R_{\max}$ the entries are the geometric mean in kilometers and the logarithmic standard deviation. (b) Eigenvalues and eigenvectors of the correlation matrix.

	Distribution		Correlation matrix				
(a)	Mean	Std dev	Z_1	Z_2	Z_3	Z_4	Z_5
$Z_1(V_{\max})$	36.7	13.7	1.000	−0.398	−0.018	−0.468	0.561
$Z_2(\ln R_{\max})$	39.3	0.53	−0.398	1.000	0.200	0.454	−0.602
$Z_3(\varphi)$	23.9	6.15	−0.018	0.200	1.000	0.278	−0.115
$Z_4(X_1)$	242.9	141.3	−0.468	0.454	0.278	1.000	−0.424
$Z_5(n)$	0.79	0.34	0.561	−0.602	−0.115	−0.424	1.000
(b) Eigenvector	**E**1		**E**2	**E**3		**E**4	**E**5
Eigenvalue	2.518		1.026	0.625		0.495	0.335
$Z_1(V_{max})$	0.470		−0.346	−0.450		0.505	−0.449
$Z_2(\ln R_{max})$	−0.497		−0.012	−0.598		0.372	0.507
$Z_3(\varphi)$	−0.197		−0.896	−0.014		−0.392	0.057
$Z_4(X_1)$	−0.474		−0.184	0.565		0.602	−0.244
$Z_5(n)$	0.518		−0.207	0.346		0.300	0.692

the subset excluded from each pair. In Part I, comparison of histograms of wind speed for both dependant and bootstrap data showed that the Holland profile exaggerated the occurrence of wind speeds >50 m s^{-1} by 20%–50%. The Holland profile also overstated the occurrence of winds <10 m s^{-1} and understated that of winds between 20 and 40 m s^{-1}.

With dependant data (Fig. 7a), in which the parameters are applied on a profile-by-profile basis to the data from which they were computed, the single-exponential profile also overestimates the occurrence of winds >40 m s^{-1}, but by <10%. For weaker winds, over- and underestimation are mixed, with some preponderance of the latter. With dependant-data linear modeling of the parameters based upon all profiles that passed QC, the pattern is much the same, although occurrences of winds >70 m s^{-1} and <10 m s^{-1} are underestimated. Linearly modeled bootstrap parameters applied to the complete dataset (Fig. 7b) are consistent with the dependant-data results, but understate the occurrence of weak winds to a somewhat greater extent. Use of mean values of the parameters greatly overstates the frequency of winds >40 m s^{-1}. Thus, while the sectionally continuous, single-exponential profile fixes some of the Holland profile's limitations, there is still room for improvement.

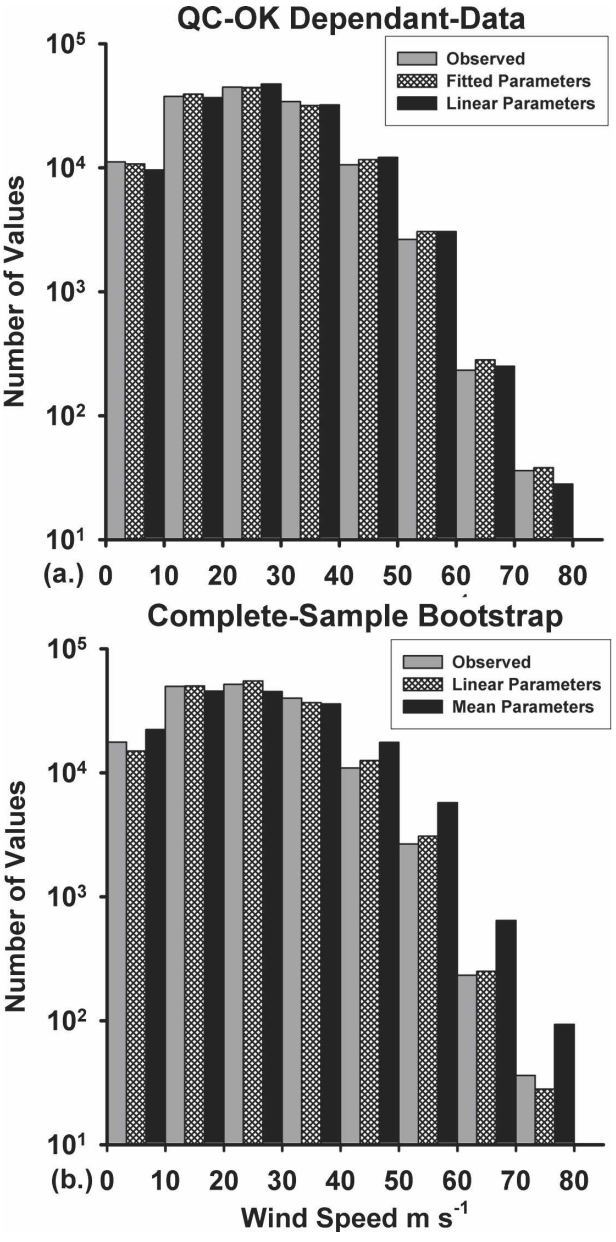

FIG. 7. Histograms of wind speed for observed and single-exponential profiles: (a) dependant-data observed (gray), computed from profile-specific fitted parameters (cross-hatched), and computed from linearly estimated parameters for profiles that passed QC (black). (b) Complete-sample observed (gray), computed from linearly estimated parameters (cross-hatched), and computed from sample mean parameters (black). Both (a) and (b) use observed radius of maximum wind.

4. Dual-exponential profiles

Although the principle of least hypothesis makes the single-exponential profiles seem attractive, their tendency toward a too-gradual radial decrease of wind with increasing radius just outside the eyewall and a too-rapid decrease at large radius, their systematic underestimation of the geopotential height fall from the vortex surroundings to center, and their overstating of the frequency of very strong and very weak winds, lead us to seek alternatives. The simplest option is inclusion of a second exponential in the outer vortex. Our original idea was to include a fixed slowly decaying exponential in order to flatten the profile at large radius and then determine the faster decay length and its relative contribution with the fitting algorithm. The difficulty with this strategy lies in the ambiguous separation between the roles of the two exponentials in the cost-function minimization algorithm. Section 5 summarizes both this formulation and one where both decay lengths are determined variationally.

After some experimentation, we found that the best version of (4) employed these outer-vortex parameters: X_2, the fixed rapid decay length, X_1, the fitted slower decay length, and A, the fitted contribution of the faster exponential to the profile. Subjective tuning showed that a wider transition, 25 km instead of 10 km, was required to avoid understating the frequency of the strongest winds with this formulation. Since smaller values of X_2 produced smaller rms differences between the observed and fitted wind profiles and smaller relative contributions by X_2 to the fitted profile, we selected the

most rapid decay length that seemed physically reasonable, 25 km, and applied a Lagrange multiplier constraint to keep $X_1 \geq 100$ km. The upper bound on X_1 was adjusted experimentally to bring the average value of $(Z_e - Z_a)$ close to zero (Fig. 8a). The value that met this criterion was $X_1 \leq 450$ km. As the upper constraint on X_1 relaxed, the average value increased (Fig. 8b), but A remained essentially constant (Fig. 8c). The average fitted values of n, X_1, and A are 0.85, 288.5 km, and 0.10. The rms and bias wind and height differences between the fitted and observed profiles are 2.03 m s^{-1}, -0.07 m s^{-1}, 11.1 m, and 1.15 m. These values were relatively insensitive to the upper bound on X_1 provided that it was >400 km. Thus, use of two exponentials reduces the rms wind error by about 20% relative to the single-exponential formulation, but reduces the wind bias and height errors by only a small amount. Because the faster decay length can fit the rapid decrease of wind speed outside the eyewall, the fitting algorithm usually selects a larger value of X_1 for the dual-exponential profile than it did with the single-exponential profile. Thus, stronger winds that extend farther from the center and integration of (5) to 1200-km radius can produce zero average difference between the calculated and climatologically expected environmental geopotential height.

In only 167 of the cases that passed QC did the fitting algorithm select $A > 0$. In the other 326 cases—about 2/3 of the total—$A = 0$ produced the smallest S^2 so that the single-exponential fit was superior to the dual-exponential fit. The average nonzero value of A was 0.26. Cyclones with nonzero A were stronger, average $V_{max} = 43.8$ m s^{-1}, compared to those with $A = 0$, average $V_{max} = 33.1$ m s^{-1}.

Despite the relatively small improvement in wind errors, the qualitative appearance of many fitted profiles was more realistic. In Hurricane Anita, where the algorithm selected $X_1 = 301$ km and $A = 0.41$, the fitted and observed profiles are virtually identical (Fig. 9), whereas the single-exponential fit with $X_1 = 100$ km was only slightly better than the corresponding Holland fit. For Hurricane Mitch (Fig. 10a), the dual-exponential fit selected $X_1 = 156$ km and $A = 0.14$. The new X_1 was only 30% larger than the corresponding single-exponential value, but the dual-exponential fit was noticeably better beyond 40-km radius. In both Hugo (Fig. 10b) and Edouard (Fig. 10c), the fitting algorithm chose $A = 0$. The single-exponential fit was optimum in these cyclones and the fitted profiles were identical to those shown in Fig. 5, apart from the effect of the wider transition zone. For Erika (Fig. 10d), the algorithm again chose a relatively small value of $A = 0.13$, and a relatively larger value of $X_1 = 318$ km, approximately

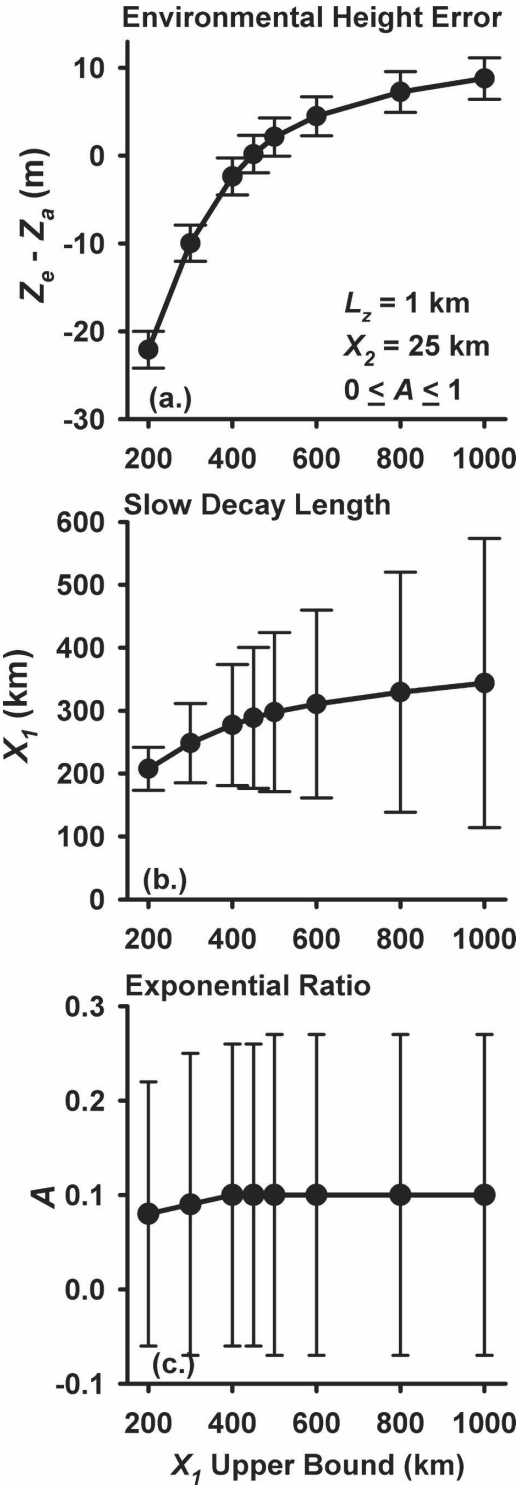

FIG. 8. Variation of (a) difference between computed and climatological environmental geopotential heights, (b) outer exponential decay length, and (c) fraction of the profile contributed by the shorter exponential with 25-km decay length as functions of the Lagrange multiplier constraint on the maximum longer decay length for dual-exponential profiles.

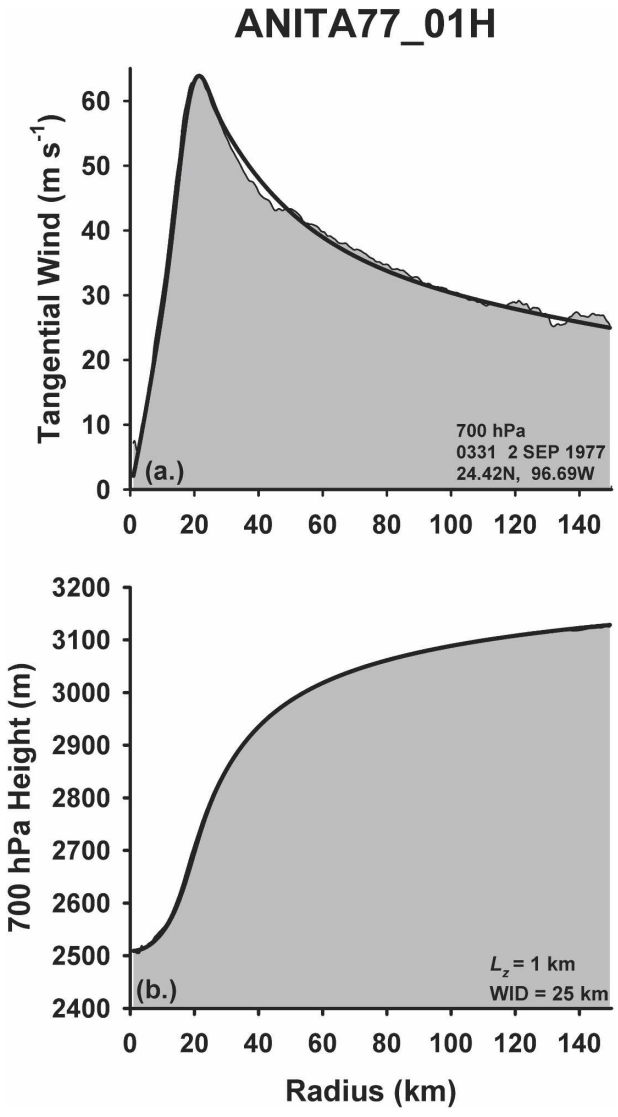

FIG. 9. Dual-exponential (a) wind and (b) geopotential height profiles fitted to Hurricane Anita of 1977. Observed and fitted profiles are as indicated in Fig. 2.

double the single-exponential value in Fig. 5. Figures 9 and 10 are typical of the dual-exponential fits. For some hurricanes, generally those with $V_{max} > 55$ m s^{-1}, nonzero values of A produce substantially more realistic fits. For some weaker hurricanes, values of A between the sample average and zero produce incremental improvements. A key advantage of this formulation is that the fitting algorithm can select $A = 0$ for cyclones where the single-exponential fit is optimum, as illustrated for Hugo and Edouard.

Scatter diagrams of A, X_1, and n as functions of V_{max} are consistent with this interpretation. Values on a regression line fitted to X_1 decrease from 352 to 211 km as V_{max} increases from 5 to 75 m s^{-1}. Although few values of X_1 are limited by the Lagrange multiplier minimum constraint 100 km $\leq X_1$, ~25% of them cluster along the maximum constraint $X_1 \leq 450$ km (Fig. 11a). The reason for this difference from the single-exponential case (Fig. 6) lies in the tighter constraint and the dual-exponential profiles' ability to represent sharp gradients near the eyewall with the X_2 part of the profile while representing the outer vortex with larger values of X_1. Nonzero values of A correspond to partial projection onto the X_2 component (Fig. 11b). The regression line for this parameter is not allowed to extend to negative values so that $A = 0$ for $V_{max} \leq 20$ m s^{-1} and increases to 0.29 at $V_{max} = 75$ m s^{-1}. Still, in roughly two-thirds of the sorties, $A \simeq 0$, so that the single-exponential profile is actually the optimum fit, as discussed above and illustrated in Figs. 9 and 10. The exponent of the power-law profile inside the eye is a bit larger than in the single-exponential profile because of the wider transition region (Fig. 11c). Only about 4% of the values are greater than two, but >70% of them are <1.

The parameter correlation matrix (Table 2a) is for the most part consistent with that for the single-exponential and Holland profiles. Here, A, X_1, and n play the same role as B in the Holland profile. The leading eigenvector, which explains >40% of the standardized parameter variance, is the same as the one recognized in the previous situations. It describes sharpening of the wind maximum and shrinking of the radius of maximum wind in more intense tropical cyclones—the convective ring phenomenon. This eigenvector has a larger eigenvalue than the corresponding single-exponential eigenvector, but it explains less of the variance because the total standardized parameter variance is 6 instead of 5. A key difference between the single- and dual-exponential profiles is the stronger projection of this eigenvector onto A and n compared with X_1. The second eigenvector describes simultaneous reduction in X_1 and A associated (weakly) with increasing intensity. It may reflect the nonuniqueness inherent in approximation of curves by sums of exponentials. That is, a smaller variable decay length with less contribution from the fixed decay length may fit a given profile just as well as a larger variable decay length with more contribution from the fixed exponential. The third eigenvector is the same as the second eigenvector identified in the Holland and single-exponential cases. It projects almost entirely onto latitude. Together, these first three eigenvectors explain nearly 80% of the parameters' standardized variance.

As in the single-exponential case, the correlations in Table 2a yield linear regression relations to predict

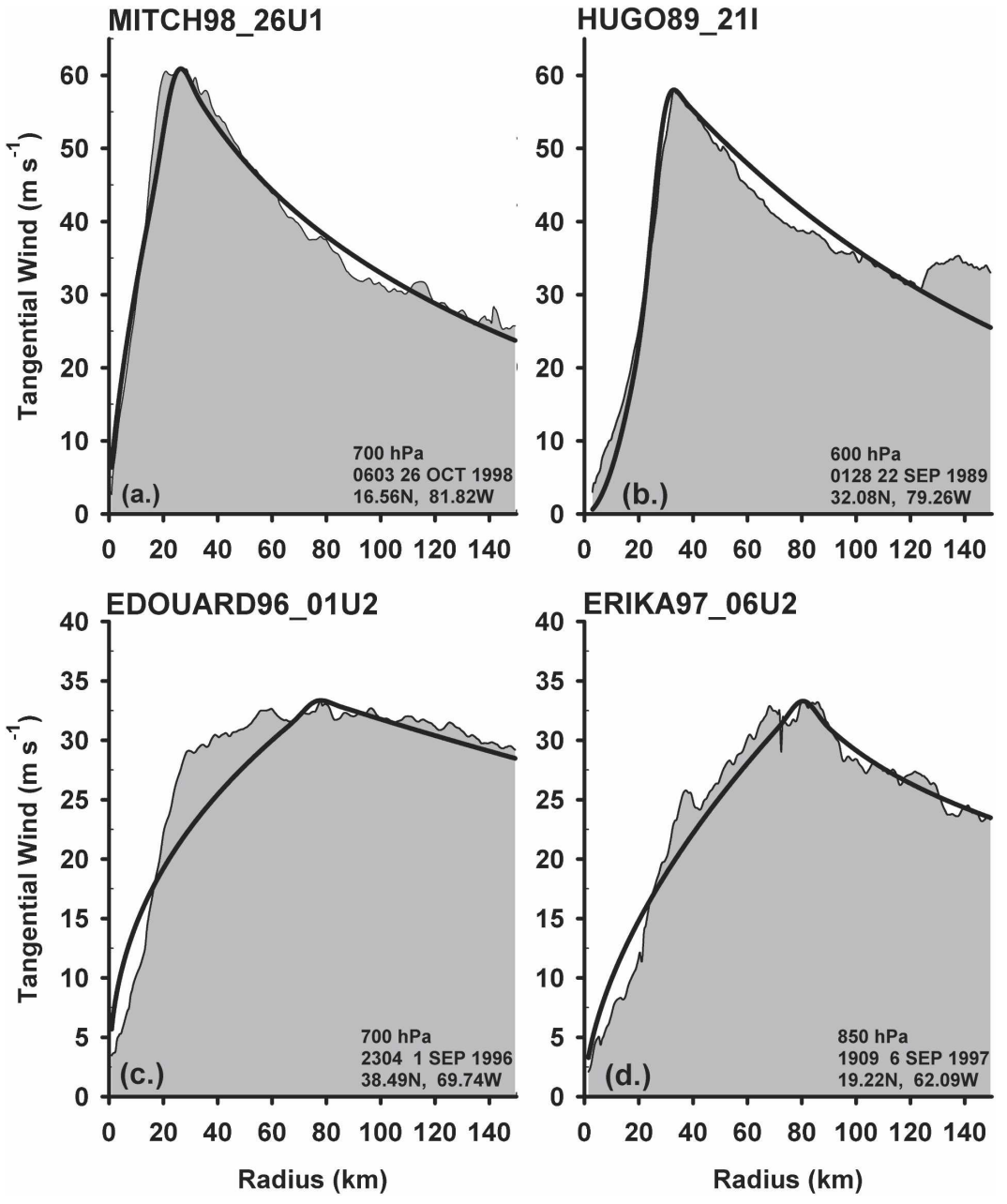

FIG. 10. Dual-exponential wind profiles fitted to Hurricanes (a) Mitch of 1998, (b) Hugo of 1989, (c) Edouard of 1996, and (d) Erika of 1997. Observed and fitted profiles are as indicated in Fig. 2.

$\ln R_{max}$, n, X_1, and A based upon knowledge of the variables that characterize hurricanes in the HURDAT file, V_{max} and φ. Since the regression relation for R_{max} is identical with (7a), it is not repeated here,

$$X_1 = 317.1 - 2.026V_{max} + 1.915\varphi, \quad (10a)$$

$$n = 0.4067 + 0.0144V_{max} - 0.0038\varphi, \quad (10b)$$

$$A = 0.0696 + 0.0049V_{max} - 0.0064\varphi, \ (A \geq 0). \quad (10c)$$

The coefficients in (10a)–(10c) differ from zero at better than 1% significance, except for the last (φ) coefficients in (10a) and (10b), which are significant at 1.4% and 16%, respectively. Alternative regression relations that use radius of maximum wind as an independent variable in addition to maximum wind and latitude are

$$X_1 = 287.6 - 1.942V_{max} + 7.799 \ln R_{max} + 1.819\varphi, \quad (11a)$$

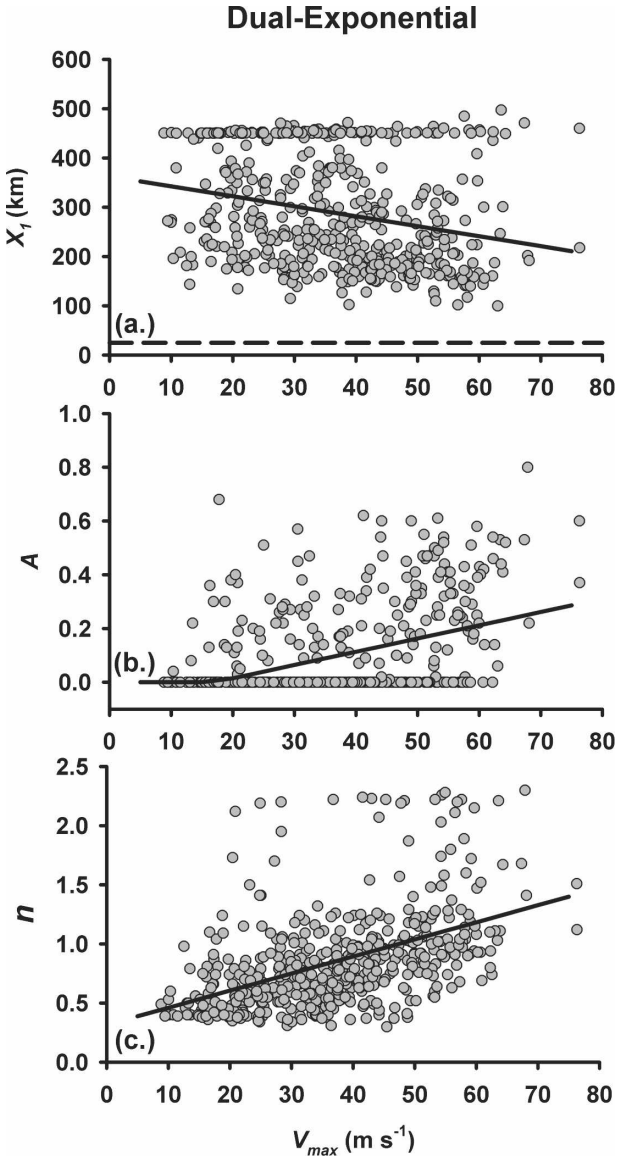

FIG. 11. Scatterplots and regression lines as functions of maximum wind for fitted (a) dual-exponential longer (solid) and shorter (dashed, fixed at 25 km) decay lengths, (b) fraction that the shorter decay length contributes to the outer profile, and (c) inner vortex power-law exponent. Shaded circles represent parameter values determined by the fitting algorithm.

$$n = 2.1340 + 0.0077V_{\max} - 0.4522 \ln R_{\max} - 0.0038\varphi, \tag{11b}$$

$$A = 0.5913 + 0.0029V_{\max} - 0.1361 \ln R_{\max} - 0.0042\varphi, \quad (A \geq 0). \tag{11c}$$

As above, all of the coefficients differ from zero at better than 1%, except for the next-to-last coefficient ($\ln R_{\max}$) in (11a), 50%, and the last (φ) coefficients in (11a) and (11b), 2.5% and 8.5%, respectively. The coefficients are so different between these two sets of equations because in (10a)–(10c) variations of the dependant variables that would project onto $\ln R_{\max}$—if it were an independent variable—project instead onto $V_{\max}$ and φ through their correlations with $\ln R_{\max}$.

Here we treat in more detail derivation of height–wind relations based upon the regression relations for the parameters. As in section 2, substitution from (10a)–(10c) into (5) and integrating to 1200-km radius produces $Z_e - Z_c$ as a function of $V_{\max}$. Algebraic relations between minimum height and maximum wind are derived by fitting power-law expressions to the resulting tabular data:

$$V_{\max} = 0.929(Z_e - Z_c)^{0.659}, \quad (\varphi = 15°\text{N}), \tag{12a}$$

$$V_{\max} = 0.661(Z_e - Z_c)^{0.701}, \quad (\varphi = 25°\text{N}), \tag{12b}$$

$$V_{\max} = 0.508(Z_e - Z_c)^{0.730}, \quad (\varphi = 35°\text{N}), \tag{12c}$$

$$V_{\max} = 0.410(Z_e - Z_c)^{0.752}, \quad (\varphi = 45°\text{N}), \tag{12d}$$

$$V_{\max} = 2.20\sqrt{Z_e - Z_c}\ (\text{mean } \ln R_{\max}, \varphi, n, X_1, \text{and } A). \tag{12e}$$

Although the coefficients in these relations vary considerably, the predicted values are surprisingly consistent, both with each other and with observed $V_{\max}$ as a function of $Z_e - Z_c$ (Fig. 12). The mean and rms errors for the complete dataset computed with (12a)–(12d) using data stratified by 10° latitude bands are 0.85 ± 5.92 m s^{-1}. With the data pooled and the square root relationship (12e), the error is 1.48 ± 5.87 m s^{-1}. These errors are essentially the same as those with the dependant-data height–wind relations fitted to the complete dataset in Part I. Not surprisingly, (12e), the mean-parameter height–wind relation overestimates the maximum wind in weaker tropical cyclones and underestimates it in stronger ones because it fails to account for the statistical sharpening of the profile with intensity. The scatter of the actual maximum winds as a function of height difference is greater than can be accounted for by latitude differences in (12a)–(12d), and much of it is due to random variations of the parameters not captured by the regression relations. The errors from (12a)–(12d) are significantly smaller than the corresponding errors with the Holland profile using linearly estimated B in Part I, −2.53 ± 6.48 m s^{-1}. From the combined analysis here and in Part I, it appears difficult to derive a height–wind relationship that can estimate maximum wind with an rms error appreciably smaller than 6 m s^{-1}.

Dependant-data histograms of the observed and fit-

TABLE 2. (a) Mean, std dev, and correlation matrix for the dual-exponential profile variables computed with X_2 fixed at 25 km from the 493 sorties that passed QC screening. For R_{max} the entries are the geometric mean in kilometers and the logarithmic std dev. (b) Eigenvalues and eigenvectors of the correlation matrix.

	Distribution		Correlation matrix					
(a)	Mean	Std dev	Z_1	Z_2	Z_3	Z_4	Z_5	Z_6
$Z_1(V_{max})$	36.7	13.7	1.000	−0.398	−0.018	−0.254	0.479	0.421
$Z_2(\ln R_{max})$	39.3	0.53	−0.398	1.000	0.200	0.152	−0.667	−0.572
$Z_3(\varphi)$	23.9	6.15	−0.018	0.200	1.000	0.112	−0.065	−0.251
$Z_4(X_1)$	288.5	112.0	−0.254	0.152	0.112	1.000	−0.143	0.165
$Z_5(n)$	0.85	0.42	0.479	−0.667	−0.065	−0.143	1.000	0.391
$Z_6(A)$	0.10	0.16	0.421	−0.572	−0.251	0.165	0.391	1.000
(b) Eigenvector	**E**1		**E**2	**E**3	**E**4		**E**5	**E**6
Eigenvalue	2.550		1.150	1.022	0.625		0.417	0.235
$Z_1(V_{max})$	−0.443		0.246	−0.239	0.700		−0.324	0.302
$Z_2(\ln R_{max})$	0.536		0.054	−0.003	0.432		−0.348	−0.663
$Z_3(\varphi)$	0.180		0.150	−0.907	−0.066		0.338	−0.061
$Z_4(X_1)$	0.135		−0.835	−0.270	0.001		−0.382	0.255
$Z_5(n)$	−0.504		0.087	−0.214	−0.466		−0.520	−0.451
$Z_6(A)$	−0.460		−0.457	0.027	0.317		0.493	−0.484

ted-profile winds show gratifying agreement (Fig. 13a) using both profile-specific parameters and linearly estimated parameters. The only noticeable problems are overestimation of the frequency of winds between 60 and 70 m s^{-1} and underestimation the frequency of winds between 70 and 80 m s^{-1} by ~10%. Bootstrap validation with linearly estimated parameters (Fig. 13b) increases the overestimation of wind occurrence in the 60–70 m s^{-1} bin, causes underestimation in the <10 m s^{-1} bin, and reduces the error in the 70–80 m s^{-1} bin. Consistent with the Holland and single-exponential experience, average values of the parameters overestimate occurrences on both the high- and low-speed tails of the wind distribution.

5. Discussion

a. Other formulations

Two other ways to fit dual exponentials to the outer-profile data involve setting X_2 to a fixed value of 300–500 km and searching variationally for A and X_1 with the latter parameter limited to values <25–150 km. This approach has five parameters, the same number as in section 3. Alternatively, both X_1 and X_2 may be sought through a free dual-exponential variational search. This approach has a total of six parameters: V_{max}, R_{max}, n, X_1, A, and X_2, four of which must be sought with the fitting algorithm. Both of these approaches are compromised by the proliferation of potentially spurious correlations among parameters and the multiple ways that different combinations of parameters can fit the same data equally well.

Figure 14 shows scatter diagrams of the free dual-exponential outer-vortex parameters with Lagrange multiplier constraints $100 \le X_1 \le 450$ and $25 \le X_2 \le 75$ km. Because the constrains are "soft" in the sense that

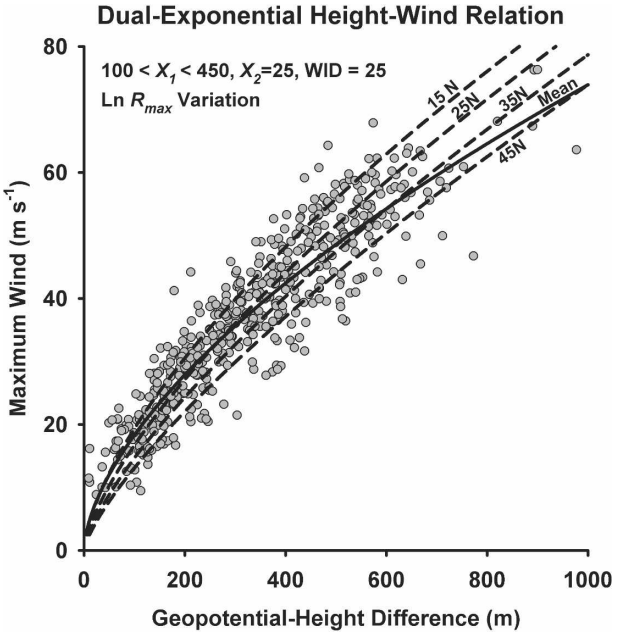

FIG. 12. Height–wind relation computed from the dual-exponential profiles. Shaded circles represent observed wind speed as a function of the difference between climatological environmental geopotential height and observed central geopotential height. Dashed curves are power-law approximations (12a)–(12d) to the height difference computed from the gradient-wind relation using parameters estimated linearly from maximum wind and latitude at 15°, 25°, 35°, and 45°. The solid curve is the height–wind relation (12e) computed with the sample-mean values of the parameters.

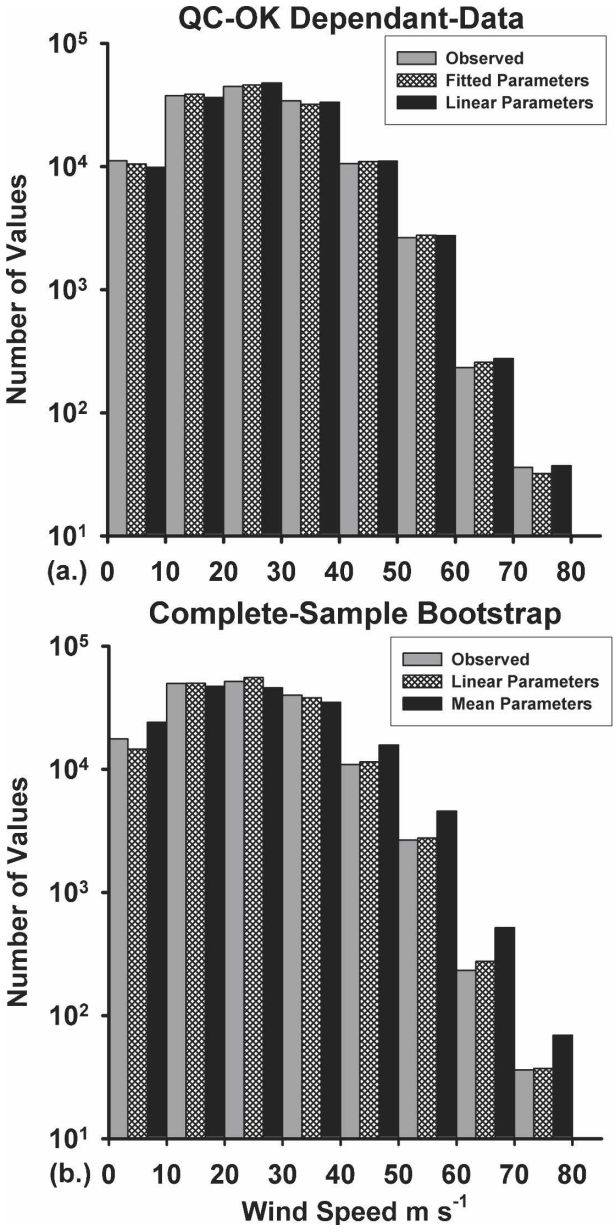

FIG. 13. Histograms of wind speed for observed and dual-exponential profile with $X_2 = 25$ km: (a) dependant-data observed (gray), computed from profile-specific fitted parameters (cross-hatched), and computed from linearly estimated parameters for profiles that passed QC (black). (b) Complete-sample observed (gray), computed from linearly estimated parameters (cross-hatched), and computed from sample mean parameters (black). Both (a) and (b) use observed radius of maximum wind.

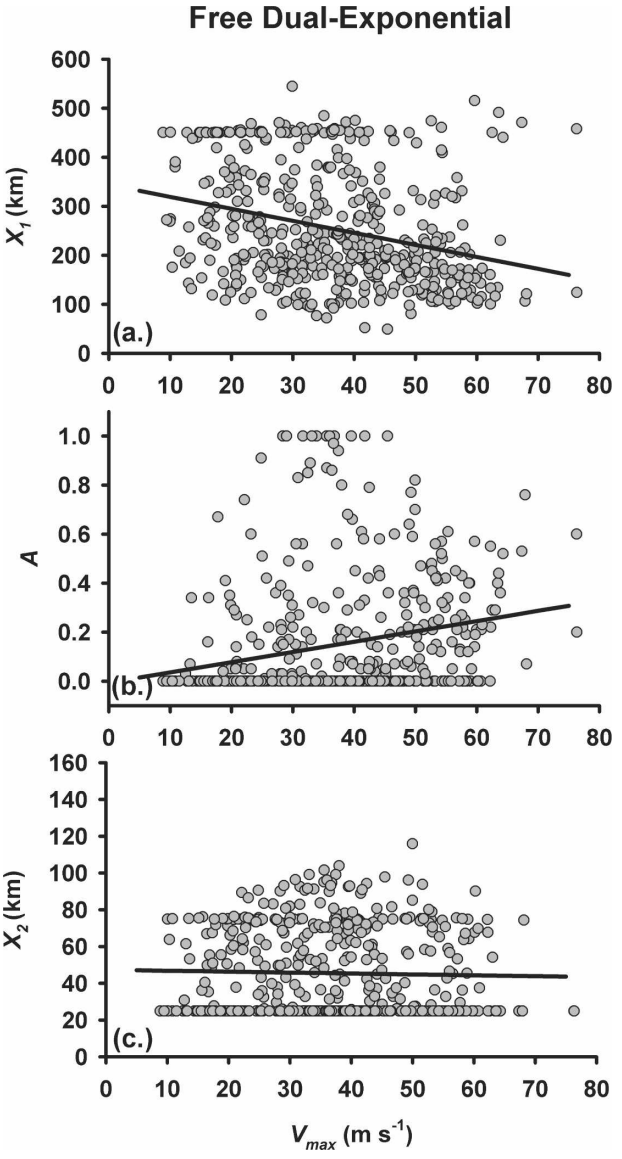

FIG. 14. Scatterplots and regression lines as functions of maximum wind for fitted (a) free, dual-exponential, longer decay length, (b) fraction that the shorter decay length contributes to the outer profile, and (c) free, dual-exponential, shorter decay length. Shaded circles represent parameter values determined by the fitting algorithm.

they impose cost-function penalties without prohibiting values outside the preferred subdomains, the fitting algorithm was able to select a few values that violate the foregoing inequalities. The regression relation for X_1 behaves much as it did in section 3, decreasing from >300 km to <200 km as V_{max} increases from 5 to 75 m s^{-1} (Fig. 14a). About 14% of values are limited by the 450 m s^{-1} upper Lagrange multiplier constraint, and unlike the analysis in section 3, about 2% are limited by the lower constraint; A on the other hand behaves differently (Fig. 14b). Only 55% of the values are zero, implying that here single-exponential fits are optimum in somewhat fewer cases than previously. The algorithm also produces ~2% of cases with $A = 1$, implying that in those cases X_2, which is constrained within the domain $25 \leq X_2 \leq 75$ km, can completely

describe the vortex outside the eye. Despite the lack of a consistent pattern in the dual-exponential fit, its regression relation for A is similar to that for the dual-exponential fit with fixed $X_2 = 25$ km, but without the identically zero values when the previous regression line was negative for $V_{max} < 20$ m s^{-1}. The X_2 scatter diagram shows erratic variation. About 47% of the X_2 values are at the lower Lagrange multiplier limit, 25 km, so that the fits to these profiles are the same as in section 3. Another 18% of the X_2 values are >75 km where they are significantly penalized by the upper X_2 constraint. These instances reflect ambiguity as the roles of the longer and shorter decay lengths overlap.

As a consequence, the regression line describes X_2 as a constant value of ~45 km, independent of V_{max}. Despite the additional degrees of freedom, the free dual-exponential fit has larger rms wind and height errors, 2.81 m s^{-1} and 12.20 m, compared with 2.03 m s^{-1} and 11.06 m with X_2 fixed at 25 m s^{-1}. A similarly vexing ambiguity arises with the shorter decay length when one attempts to fit it, A, and a fixed longer decay length. The reason for these problems lies in local minima of the cost function that are distinct from the global minimum. Perhaps insightful application of different constraints and a more sophisticated minimization algorithm can resolve these issues, but for now, the dual exponential profile with a fixed shorter decay length seems to be the simplest representation of the data.

b. Vortex stability

Since one potential application of these profiles is theoretical studies of vortex dynamics, it is useful to explore their hydrodynamic stability properties. Figure 15 shows the absolute vorticity and angular velocity for the dual-exponential profile fitted to Hurricane Anita (Fig. 9). The vorticity is everywhere >0 so that the profile is inertially stable. It exhibits a relative minimum at the center and a pronounced maximum just inside the radius of maximum wind so that it meets the necessary condition for barotropic instability (e.g., Schubert et al. 1999). The vortex angular velocity also exhibits a maximum that causes the algebraically growing wavenumber-1 instability described by Nolan and Montgomery (2000). The vorticity and angular velocity maxima in Anita arise primarily because $n > 1$, but the way that the outer and inner profiles overlap in the transition zone can produce local maxima of these quantities near the eyewall even when $n < 1$, but not when it is significantly smaller than unity. When $n < 1$, the power-law profile has infinite angular velocity and vorticity at the center (Fig. 16a) if it is continued to $r = 0$. Difficulty with the singularity can be avoided in these

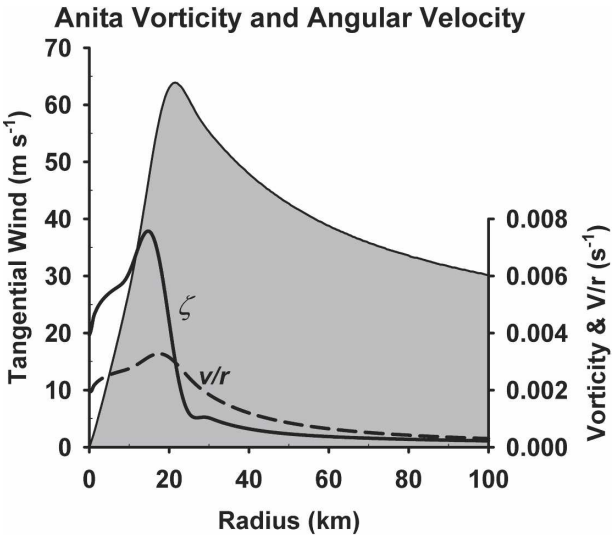

FIG. 15. Vorticity (solid) and angular velocity (dashed) for the dual-exponential profile with $X_2 = 25$ km fitted to Hurricane Anita of 1977. Here, the fitted wind profile is the shading boundary.

cases by replacing the power-law wind profile with $V_i' = (L_c\zeta_c/2)[r/L_c - (r/L_c)^3/2]$, which is derived from a parabolic radial vorticity distribution, $\zeta = \zeta_c[1 - (r/L_c)^2]$ for $r \le L_c$ and $\zeta = 0$ for $r > L_c$. This vorticity distribution by itself would support a Rankine-like vortex with free-vortex flow proportional r^{-1} outside the core (Fig. 16b). Here L_c is chosen such that the ratio of the inner profile vorticity at R_{max} to that at $R_{max}/4$ is the same as in the power-law vortex, $\zeta(R_{max})/\zeta(R_{max}/4) = (1/4)^{1-n}$. Then ζ_c is chosen such that $V_i'(R_{max}) = V_{max}$.

This formulation removes the central singularity and produces a monotonic outward decrease of vorticity when $n \le 0.55$ (Fig. 16c). The vorticity decreases steadily from the center outward, as in the regime 1 profiles described by Kossin and Eastin (2001). Larger values of n model their regime 2 profiles. The transition between the two regimes happens over the range $0.55 < n < 1$. When $n \le 0.8$, the V_i increases more gradually with radius near $r = R_{max}$, and (3) shows that the relative contribution of V_o to the outer profile shape at and inside R_{max} is smaller. For smaller n, the smooth decrease and lack of a vorticity singularity at the origin make these composite, parabolic vorticity profiles more suitable for theoretical studies than the fitted power-law profiles, although the fitted profiles are adequate for studies of hurricane impacts.

Dual-exponential profiles often exhibit a relative vorticity minimum in the strong anticyclonic shear just outside the eye. This feature occurs where the fitted profiles match the data closely. It is a consequence of the modeled rapid decrease of the wind around the eye

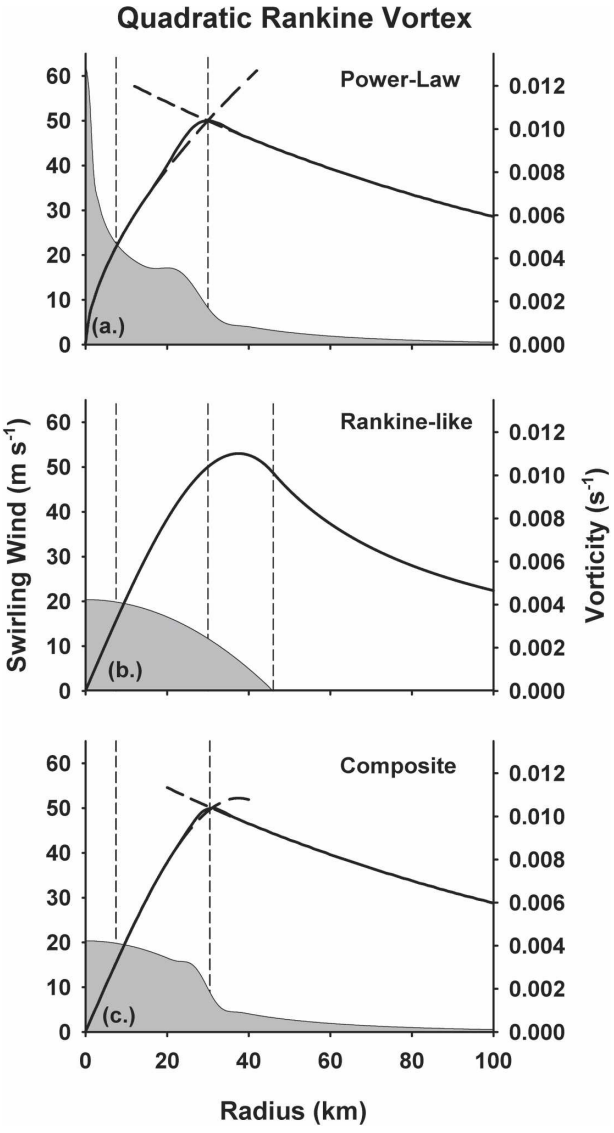

FIG. 16. (a.) Single-exponential profile with $n = 0.6$ and $X_1 = 125$ km. (b) Rankine-like vortex induced by a quadratic-parabola vorticity distribution. The vorticity in (b) matches that in (a) at R_{max} and $R_{max}/4$. (c) Composite vortex where the velocity distribution inside the eye is replaced by the Rankine-like vortex. The solid curve is the wind. The dashed curves are the inner and outer wind profiles, and the shading indicates the vorticity distribution.

and the more gradual decease in the outer part of the vortex. It raises the possibility that intense hurricanes become barotropically unstable at the end of an episode of rapid deepening more or less at the time when outer wind maxima normally form.

6. Conclusions

The dual-exponential profiles presented here provide an observationally based representation of the structure of the hurricane vortex to support such diverse undertakings as theoretical vortex dynamics, storm-surge forecasting, and windstorm loss modeling. The statistical estimates of the parameters given by (7a), (10a)–(10c), and (11a)–(11c) allow construction of axisymmetric hurricane vortices using (1a)–(1c) and (4). The resulting wind variations are consistent with a large sample of aircraft observations and have latitude-dependant height–wind relations (12a)–(12d). Although these relations take into account the statistical sharpening of the wind maximum in more intense tropical cyclones, maximum winds computed from them have an inherent uncertainty of ~ 6 m s^{-1}. Outer vortex exponential decay lengths >200 km are consistent with the argument of Mallen et al. (2005) that real hurricanes are relatively broad vortices well able to resist the effects of environmental shear. An alternative vortex structure with only one exponential does not capture the rapid decrease of the wind outside the eye of the most intense hurricanes, although it can represent weaker hurricanes adequately. Single-exponential profiles also fail to match the average isobaric height difference from the vortex periphery to center. For $n < 1$, replacement of the power-law profile inside the eye with one derived from a parabolic vorticity distribution produces analytical vortices more suitable for theoretical studies of hurricane dynamics.

A key limitation of this study is exclusion of tropical cyclones that failed to meet the QC criteria because they had large radii of maximum wind. Reanalysis, including hurricanes that have occurred since the 2000 season, as well as using different QC criteria and different Lagrange multiplier constraints, promises to improve this situation. Other unfinished work is calibration of the axisymmetric maximum wind in terms of the HURDAT climatology and inclusion of secondary wind maxima in the statistical representation.

Acknowledgments. Our coauthor, Ed Rahn, died in November 2004 as we were finalizing this paper. His meticulous analysis of aircraft data and formidable programming talent were cornerstones of this work. He was a good friend and colleague who will be missed.

We are grateful to scientists, flight crew, and ground support staff in NOAA and the Air Force. Without their skill and dedication to the difficult and demanding task of flying into hurricanes, this research would not have been impossible. The acquisition and maintenance of the data archive was supported by Hurricane Research Division base funds, and HEW's efforts since December 2002 were supported by Florida International University research discretionary funds and NSF Grant ATM-0454501. We thank Kevin Mallen for his

insightful comments and Sneh Gulati for statistical advice.

APPENDIX

Bellramp Functions

In section 2, the transition between the outer exponential profile and the inner power-law profile was accomplished with a polynomial that superficially resembled a hyperbolic tangent, but had finite width and increased smoothly from zero to one as its nondimensional argument, ξ, also increased from zero to one. This polynomial "ramp function" was derived by integration of a polynomial "bell function" of the form

$$b_k(\xi) = 0, \quad (\xi \le 0 \quad \text{or} \quad 1 \le \xi), \tag{A1a}$$

$$b_k(\xi) = C_k[\xi(1 - \xi)]^k, \quad (0 \le \xi \le 1). \tag{A1b}$$

Here k is the order of the bell function, although b_k is a polynomial of order $2k$. The $k - 1$st derivative of b_k is the highest derivative that remains continuous at $\xi = 0$ and $\xi = 1$. Thus, for b_1 only the function itself is continuous; for b_2 the function and first derivative are continuous; and so forth. As shown below, the bell curves become narrower with increasing order; $[\xi(1 - \xi)]^k$ has maximum value on $(0 \le \xi \le 1)$ of 2^{-2k} at $\xi = 1/2$ so that setting $C_k = 2^{2k}$ would produce bell functions with unit amplitude.

A more interesting alternative involves integration of b_k from zero to one and selection of C_k to make the area under the bell curve unity. Here are the $k = 1$ through 4 ramp functions produced by integration of $b_1(\xi)$ through $b_4(\xi)$ in a form convenient for numerical calculation:

$$w_1(\xi) = \xi^2(3 - 2\xi), \tag{A2a}$$

$$w_2(\xi) = \xi^3[10 - \xi(15 - 6\xi)], \tag{A2b}$$

$$w_3(\xi) = \xi^4\{35 - \xi[84 - \xi(70 - 20\xi)]\}, \tag{A2c}$$

$$w_4(\xi) = \xi^5\langle 126 - \xi\{420 - \xi[540 - \xi(315 - 70\xi)]\}\rangle. \tag{A2d}$$

Here (A2a)–(A2d) incorporate C_1–$C_4 = 6$, 30, 140, and 630, chosen to make $w_k(1) = 1$. By definition, $w_k(\xi) = 0$ when $\xi \le 0$, and $w_k(\xi) = 1$ when $1 \le \xi$.

Figures A1a and A1b illustrate $b_2(\xi)$ through $b_4(\xi)$ and $w_2(\xi)$ through $w_4(\xi)$, respectively. As anticipated, the bell curves become narrower, and their amplitude increases with increasing k while the transition described by w_k becomes sharper. Some of these polynomials are familiar in other contexts. For example, (A2a) is a Hermite shape function used in finite-element analysis. In the limit of very large k, b_k, and w_k, respectively, approach Dirac delta and Heaviside functions, albeit gradually. Thus, it is possible to produce highly differentiable, finite-width bell and ramp curves by the method outlined here. Because these curves are efficient to compute, they offer simple-to-use alternatives to Gaussian or hyperbolic-tangents functions for constructing forcing functions for theoretical models, representation of jet or shear flows, or patching together piecewise continuous curves as we have done here.

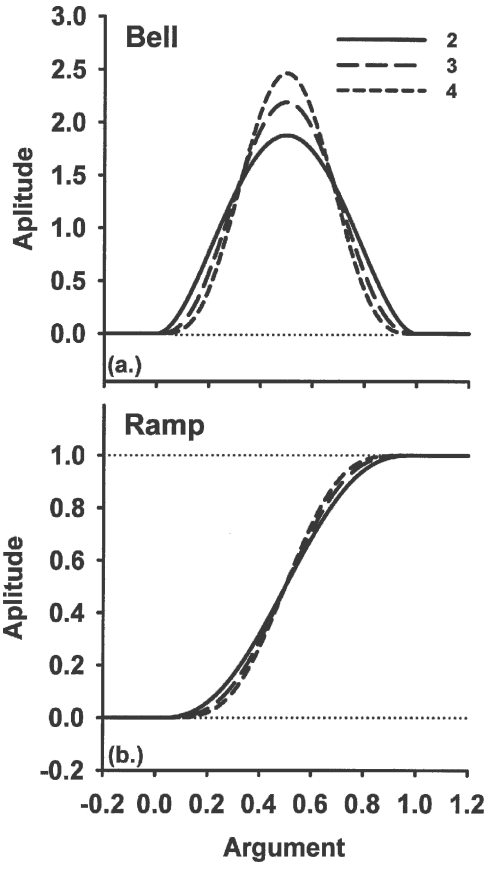

FIG. A1. Polynomial (a) bell and (b) ramp functions computed from (A1) and (A2).

REFERENCES

Atkinson, G. D., and C. R. Holliday, 1977: Tropical cyclone minimum sea level pressure/maximum sustained wind relationship for the western North Pacific. *Mon. Wea. Rev.,* **105,** 421–427.

Holland, G. J., 1980: An analytic model of the wind and pressure profiles in hurricanes. *Mon. Wea. Rev.,* **108,** 1212–1218.

Jarvinen, B. R., C. J. Neumann, and M. A. S. Davis, 1984: A tropical cyclone data tape for the North Atlantic Basin, 1886–1983: Contents, limitations, and uses. NOAA Tech. Memo.

NWS NHC 22, Coral Gables, FL, 21 pp. [Available online at http://www.nhc.noaa.gov/pastall.shtml.]

Jelesnianski, C. P., 1967: Numerical computation of storm surges with bottom stress. *Mon. Wea. Rev.,* **95,** 740–756.

Jordan, C. L., 1958: Mean soundings for the West Indies area. *J. Meteor.,* **15,** 91–97.

Kossin, J. P., and M. D. Eastin, 2001: Two distinct regimes in the kinematic and thermodynamic structure of the hurricane eye and eyewall. *J. Atmos. Sci.,* **58,** 1079–1090.

Mallen, K. J., M. T. Montgomery, and B. Wang, 2005: Reexamining the near-core radial structure of the tropical cyclone primary circulation: Implications for vortex resiliency. *J. Atmos. Sci.,* **62,** 408–425.

Nelder, J. A., and R. Mead, 1965: A simplex method for function minimization. *Comput. J.,* **7,** 308–313.

Nolan, D. S., and M. T. Montgomery, 2000: The algebraic growth of wavenumber-1 disturbances in hurricane-like vortices. *J. Atmos. Sci.,* **57,** 3514–3538.

Press, W. H., B. P. Flannery, S. A. Teukolsky, and W. T. Vettering, 1986: 10.4 Downhill simplex method in multidimensions. *Numerical Recipes: The Art of Scientific Computing,* Cambridge University Press, 289–293.

Schubert, W. H., and J. J. Hack, 1982: Inertial stability and tropical cyclone development. *J. Atmos. Sci.,* **39,** 1687–1697.

——, M. T. Montgomery, R. K. Taft, T. A. Guinn, S. R. Fulton, J. P. Kossin, and J. P. Edwards, 1999: Polygonal eyewalls, asymmetric eye contraction and potential vorticity mixing in hurricanes. *J. Atmos. Sci.,* **56,** 1197–1223.

Shapiro, L. J., and H. E. Willoughby, 1982: The response of balanced hurricanes to local sources of heat and momentum. *J. Atmos. Sci.,* **39,** 378–394.

Sheets, R. C., 1969: Some mean hurricane soundings. *J. Appl. Meteor.,* **8,** 134–146.

Smith, R. K., 1981: The cyclostrophic adjustment of vorticies with application to tropical cyclone modification. *J. Atmos. Sci.,* **38,** 2021–2030.

Vickery, P. J., and L. A. Twisdale, 1995: Prediction of hurricane wind speeds in the United States. *J. Struct. Eng.,* **121,** 1691–1699.

Willoughby, H. E., 1995: Normal-mode initialization of barotropic vortex motion models. *J. Atmos. Sci.,* **52,** 4501–4514.

——, and M. E. Rahn, 2004: Parametric representation of the primary hurricane vortex. Part I: Observations and evaluation of the Holland (1980) model. *Mon. Wea. Rev.,* **132,** 3033–3048.